Features of the molecular orbital in the photoelectron momentum distribution using elliptically polarized laser fields

Jiaqing Yan,[1] Min Li,[1,*] Wenhai Xie,[1] Chuanpeng Cao,[1] Keyu Guo,[1] Zichen Li,[1] Yueming Zhou,[1] and Peixiang Lu[1,2]
[1]*Wuhan National Laboratory for Optoelectronics and School of Physics, Huazhong University of Science and Technology, Wuhan 430074, China*
[2]*Optics Valley Laboratory, Hubei 430074, China*

(Received 20 September 2022; revised 21 November 2022; accepted 30 November 2022; published 12 December 2022)

We study the photoelectron momentum distribution from strong-field tunneling ionization of two molecules with similar highest occupied molecular orbitals, i.e., O_2 and CO_2. We find that the tiny difference between those two molecular orbitals can be clearly identified from the photoelectron momentum distributions in an elliptically polarized laser field, while it can hardly be identified in a linearly polarized laser field due to the strong Coulomb focusing effect. Furthermore, we show that the momentum distribution in the elliptically polarized laser field can be used to reveal how the molecular orbital affects the ionization time distribution of the photoelectron.

DOI: 10.1103/PhysRevA.106.062812

I. INTRODUCTION

There are many intriguing phenomena when a molecule is tunnel ionized by a strong laser field, such as suppressed ionization [1,2], resonance enhanced ionization [3,4], and laser-induced electron diffraction [5–7]. In molecular tunneling ionization, an electron is released predominantly from the highest occupied molecular orbital (HOMO). Thus the electronic structure of the HOMO can be extracted from the measured photoelectron momentum distribution (PMD). The extraction of the molecular electronic structures is of particular interest because those structures are responsible for the chemical properties of the molecule.

Previously, the PMD in the plane perpendicular to the polarization direction of a linearly polarized laser field was usually used to image the molecular orbital [5,8,9]. Because the electron momentum in this plane is not influenced by the laser electric field, the perpendicular momentum distribution of a molecule can be written as a production of a Gaussian filtering function and the electronic wave function of the molecule [10]. Using this principle, features of two very different ionizing orbitals in the PMD can be identified [5,8]. By separating the signals from the nondissociative and dissociative channels of C_2H_2, one can resolve the HOMO and the next lower-lying orbital (HOMO − 1) because those two orbitals also have different electronic structures [9]. However, it is hard to distinguish two molecular orbitals with similar electronic structures using linearly polarized laser fields.

Compared with linearly polarized laser fields, elliptically polarized laser fields provide more dimensions for the study of strong-field ionization. In an elliptically polarized laser field, the photoelectrons emitted at different instants can be mapped onto different momenta. Thus the PMD in an elliptically polarized laser field records the temporal information of the photoelectron [11–14]. Furthermore, the PMDs in elliptically polarized laser fields are much more robust against the Coulomb effect [15,16]. It is possible to distinguish two similar molecular electronic orbitals from the PMDs using elliptically polarized laser fields.

In this paper, we use an elliptically polarized laser field to ionize two prealigned molecules, i.e., O_2 and CO_2, whose HOMOs are very similar. We study the PMDs in the plane perpendicular to the major axis of the laser ellipse, and we find that the PMDs show different features for O_2 and CO_2 molecules. Those different features are caused by the small difference of the HOMOs between those two molecules. When a linearly polarized laser field is used, the PMDs become similar for those two molecules. This is attributed to the fact that the Coulomb focusing in the linearly polarized laser field is much stronger than that in the elliptically polarized laser field. Thus one might achieve a high resolution in molecular orbital imaging using elliptically polarized laser fields. Furthermore, we find that the effect of molecular orbitals on the photoelectron ionization time is recorded by the PMDs in the elliptically polarized laser field.

II. METHODS

A. Experimental setup

Our experimental setup is similar to that used in our previous experiments [13,17]. Briefly, the laser pulse (wavelength centered at 800 nm, pulse duration of ∼40 fs, repetition rate of 5 kHz) is generated by an amplified Ti:sapphire femtosecond laser system, and it is split into an alignment pulse and an ionization pulse using a beam splitter. The duration of the alignment pulse is stretched to ∼100 fs through an 8-mm-thick SF11 glass. Eventually, the alignment and ionization pulses are recombined and focused by an $f = 75$ mm parabolic mirror into an O_2 or CO_2 gas jet. The three-dimensional momenta of the resulting

*mli@hust.edu.cn

photoelectrons are detected using cold-target recoil-ion momentum spectroscopy (COLTRIMS) [18,19]. The ellipticities of the ionization pulses are $\varepsilon = 0$ and $\varepsilon \approx 0.35$ for the two cases. The peak intensity of the ionization pulses is almost 2×10^{14} W/cm^2. In our experiment, the z and y axes represent the major and minor axes of the polarization ellipse for the elliptically polarized laser pulse, respectively. For the case of linear polarization, the laser polarization direction is along the z direction. x represents the laser propagation direction.

B. Molecule alignment

In order to obtain the field-free molecular alignment, the time delays between the alignment and ionization pulses are set to be ~3.0 and ~21.2 ps for O_2 and CO_2, respectively [20]. In this paper, the molecular alignment direction is changed by rotating the polarization direction of the alignment pulse. The three-dimensional degree of alignment is $\langle \cos^2 \vartheta \rangle \approx 0.6$, which is estimated by comparing the delay-dependent yield with that by solving the time-dependent Schrödinger equation based on the rigid rotor model [13,21,22]. Here, ϑ is the angle between the molecular axis and the polarization direction of the alignment pulse. The z and y directions correspond to $\theta = 0^\circ$ and $\theta = 90^\circ$, respectively. Here, θ is the angle between the polarization direction of the alignment pulse relative to the z axis. For the cases of $\theta = 0^\circ$ and $\theta = 90^\circ$, the alignment pulse creates a rotational wave packet that results in molecules aligned primarily along the z and y axes, respectively.

C. Classical-trajectory simulation

A three-dimensional classical trajectory Monte Carlo simulation [23–26] considering the molecular orbital effect is used to interpret our experimental results. The parameters in our simulation are the same as those in the experiment. In the simulation, the electron is released at the tunnel exit position via quantum tunneling. The evolution of the electron's trajectory after tunneling is determined by the classical Newtonian equation, i.e. [atomic units (a.u.) are used in this paper unless stated otherwise],

$$\ddot{r}(t) = -E(t) - \nabla V(r), \tag{1}$$

where $E(t)$ is the laser field, $V(r) = -1/\sqrt{r^2 + a}$ is the Coulomb potential, and r is the distance between the electron and ion. a is the soft parameter, which is set to be 0.01 in this paper. The initial condition of each trajectory is given according to the partial Fourier-transform approach [27–29]. Each trajectory of the tunneling electron is weighted by

$$W(\mathbf{k}_\perp, r_0, t) \propto \left| \iint \Psi(\mathbf{r}_\perp, r_0, t) G(\mathbf{k}_\perp^2) e^{i\mathbf{k}\cdot\mathbf{r}} dr \right|^2, \tag{2}$$

where $\Psi(\mathbf{r}_\perp, r_0, t)$ is the cut of the HOMO wave function at r_0. r_0 is the matching point in the partial Fourier-transform approach [27]. $G(\mathbf{k}_\perp^2) = e^{-\frac{\kappa}{2E_0}\mathbf{k}_\perp^2}$ is the tunneling filter. $\mathbf{k}_\perp$ and $\mathbf{r}_\perp$ represent the initial momentum at the tunnel exit and the electron coordinate at the matching point perpendicular to the instantaneous electric field direction. $\kappa = \sqrt{2I_p}$ with I_p being the ionization potential. We calculate the PMDs at two alignment cases, i.e., $\theta = 0^\circ$ and $\theta = 90^\circ$, which are obtained by summing all trajectories in the photoelectron momentum plane.

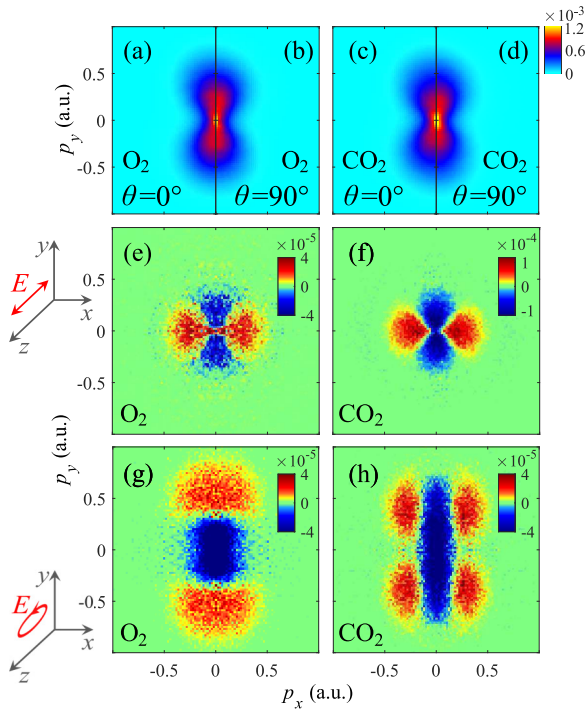

FIG. 1. (a)–(d) The measured PMDs for O_2 [(a) and (b)] and CO_2 [(c) and (d)] molecules in the elliptically polarized laser fields at $\theta = 0^\circ$ [(a) and (c)] and $\theta = 90^\circ$ [(b) and (d)]. (e)–(h) The measured NDs of the PMDs for O_2 [(e) and (g)] and CO_2 [(f) and (h)] molecules in linearly polarized [(e) and (f)] and elliptically polarized [(g) and (h)] laser fields. x is the laser propagation direction and y is the minor axis direction of the elliptically polarized laser field.

The electronic wave functions for the molecules, i.e., the HOMOs, are obtained by the calculation using an augmented correlation-consistent polarized valence triple-zeta (aug-cc-pVTZ) basis set [30,31] of the GAUSSIAN software [32]. The equilibrium internuclear distances for O_2 ($R_{\text{O-O}} = 1.30$ Å) and CO_2 ($R_{\text{C-O}} = 1.14$ Å) are obtained from the National Institute of Standards and Technology (NIST) Computational Chemistry Comparison and Benchmark Database [33].

III. RESULTS AND DISCUSSION

In Figs. 1(a)–1(d), we show the projections of the three-dimensional PMDs onto the p_x-p_y plane of O_2 and CO_2 in the elliptically polarized laser fields for $\theta = 0^\circ$ and $\theta = 90^\circ$, respectively. The PMDs looks similar for those two alignment cases. To highlight the molecular orbital effect on the PMD, we use the normalized difference (ND) of the PMDs between two alignment cases of $\theta = 0^\circ$ and $\theta = 90^\circ$ [5,9], which is given by

$$\text{ND} = M_{\theta=0^\circ} - M_{\theta=90^\circ}, \tag{3}$$

where $M_{\theta=0^\circ}$ and $M_{\theta=90^\circ}$ are the PMDs at the alignment cases of $\theta = 0^\circ$ and $\theta = 90^\circ$, respectively. Note that $M_{\theta=0^\circ}$ and $M_{\theta=90^\circ}$ have been normalized to the sum yield in the PMDs.

In Figs. 1(e)–(h), we show the measured NDs of O_2 and CO_2 in linearly and elliptically polarized laser fields. In the

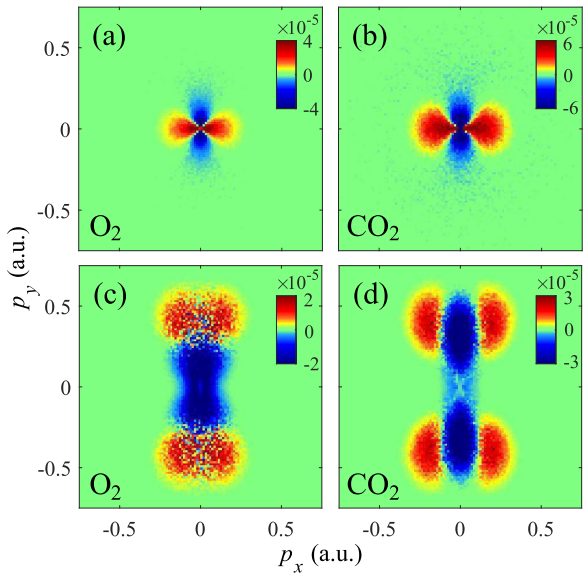

FIG. 2. (a)–(d) The same as Figs. 1(e)–1(h) but obtained by the classical-trajectory simulation. Note that the alignment averaging effect is considered in the simulation.

linearly polarized field, as shown in Figs. 1(e) and 1(f), the NDs exhibit similar patterns for O_2 and CO_2 molecules in the momentum region of $p_r = \sqrt{p_x^2 + p_y^2} < 0.5$ a.u. Those patterns were also shown in a previous study for O_2 [5], which can be explained simply. The PMD of O_2 in the plane perpendicular to the polarization direction is isotropic for $\theta = 0^\circ$ while it reveals a maximum along the p_y direction for $\theta = 90^\circ$. Therefore the subtraction of the PMDs of $\theta = 0^\circ$ and $\theta = 90^\circ$ shows a clear maximum along the p_x direction and a clear minimum along the p_y direction. The ND of CO_2 reveals nearly the same pattern as that of O_2. However, in the elliptically polarized laser field [Figs. 1(g) and 1(h)], the NDs are very different for O_2 and CO_2. Particularly, there are two maxima at $(|p_x|, |p_y|) \approx (0.0, 0.5$ a.u.) for the ND of O_2 [Fig. 1(g)], while there are four maxima at $(|p_x|, |p_y|) \approx (0.3, 0.5$ a.u.) for the ND of CO_2 [Fig. 1(h)].

We show in Fig. 2 the simulated NDs of O_2 and CO_2 in linearly and elliptically polarized laser fields using the classical-trajectory method. It should be noted that the nonadiabatic effects of the tunnel ionization were not included in our simulation [34,35], so the momentum range of the simulated results is slightly smaller than the experimental result. We can find that three clear features observed in the measured NDs are all reproduced by the classical-trajectory simulations. (i) In the elliptically polarized laser field, there are two maxima at $|p_y| \approx 0.5$ a.u. for both O_2 and CO_2 along the p_y direction, i.e., the direction of the minor axis of polarization. (ii) In the elliptically polarized laser field, the NDs reveal a clear minimum at $p_x = 0$ for CO_2, while no minimum appears for O_2 along the p_x direction. (iii) In the linearly polarized laser field, the NDs show similar patterns for the O_2 and CO_2 molecules. Next we will analyze these three features based on the classical-trajectory method.

We first study the PMD along the minor axis of polarization (p_y) of the elliptically polarized laser pulse. In the elliptically

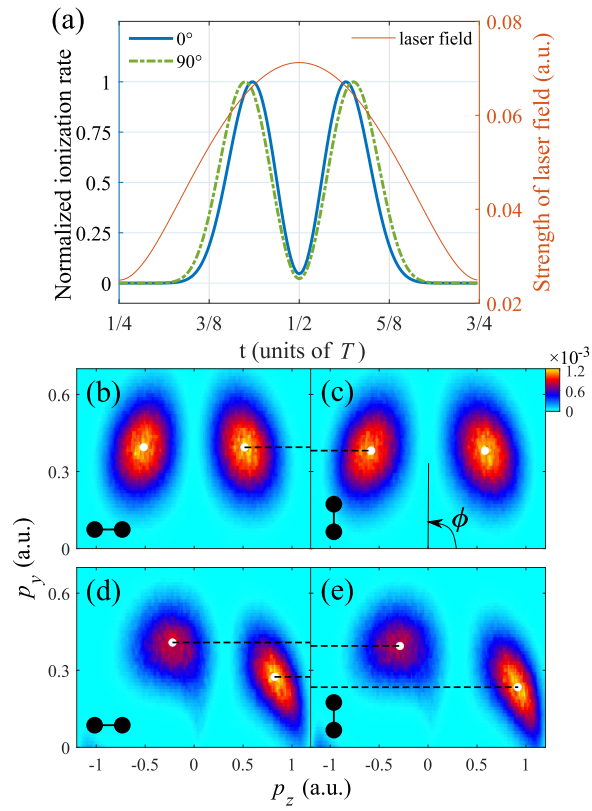

FIG. 3. (a) The ionization rate of O_2 calculated by the partial Fourier-transform approach as a function of time in the elliptically polarized laser field ($\epsilon = 0.35$) for the molecular axes along the z ($\theta = 0^\circ$) and y ($\theta = 90^\circ$) directions. For comparison, the absolute value of the electric field vector within a half laser cycle is shown by the solid orange line. (b)–(e) The simulated PMDs for the O_2 molecule in the elliptically polarized laser fields for 0° [(b) and (d)] and 90° [(c) and (e)]. Those PMDs are obtained without [(b) and (c)] and with [(d) and (e)] consideration of the Coulomb effect. The black dashes lines in (b)–(e) indicate the p_y value of the local maxima of the PMDs.

polarized laser field, the photoelectrons emitted at different instants are mapped onto different momenta in the polarization plane. Thus the PMD along the minor axis of the laser ellipse should be related to the ionization time distribution for the photoelectrons. In Fig. 3(a), we show the ionization rate of O_2 within a half laser cycle from $T/4$ to $3T/4$ (T is the period of the 800-nm laser field, and the instant of $T/2$ corresponds to the laser electric field peak) for the cases of molecular axes along the z and y directions. The instantaneous ionization rate, including the minima at $T/2$ in Fig. 3, directly reflects the orbital symmetry of the O_2 molecule, whose HOMO is a π_g orbital [20]. Due to the nodes of the HOMO, the maxima of the ionization rate for $\theta = 0^\circ$ and $\theta = 90^\circ$ do not appear at the instant of $T/2$, i.e., the field peak. Instead, the ionization rate reveals two maxima within a half laser cycle. As shown in Fig. 3, the maxima of the ionization rate at $\theta = 0^\circ$ appear at $\sim 0.436T$ and $\sim 0.564T$, which are closer to the laser electric field peak of $T/2$ than the case of $\theta = 90^\circ$ (the maxima appear at $\sim 0.425T$ and $\sim 0.575T$ for $\theta = 90^\circ$). Without considering the Coulomb effect, as shown in Figs. 3(b) and 3(c), the electron emitted at the instant of $T/2$ will be mapped onto

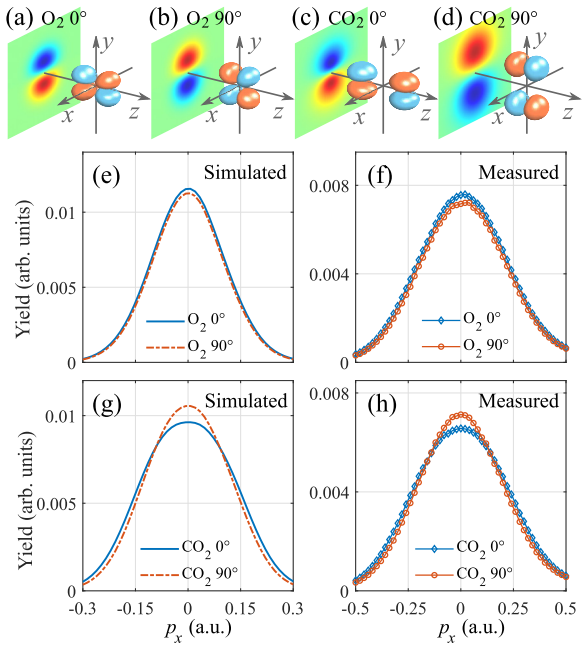

FIG. 4. (a)–(d) The HOMOs of O_2 [(a) and (b)] and CO_2 [(c) and (d)] molecules and their cuts of the wave function at the matching point of the partial Fourier-transform approach. The wave functions of (a) and (c) and those of (b) and (d) correspond to the cases of $\theta = 0^\circ$ and $\theta = 90^\circ$, respectively. (e)–(h) The simulated [(e) and (g)] and measured [(f) and (h)] final momentum distributions of O_2 and CO_2 in the laser propagation (p_x) direction of the elliptically polarized laser field ($\epsilon = 0.35$). The blue lines and the orange lines correspond to the alignment cases of $\theta = 0^\circ$ and $\theta = 90^\circ$, respectively.

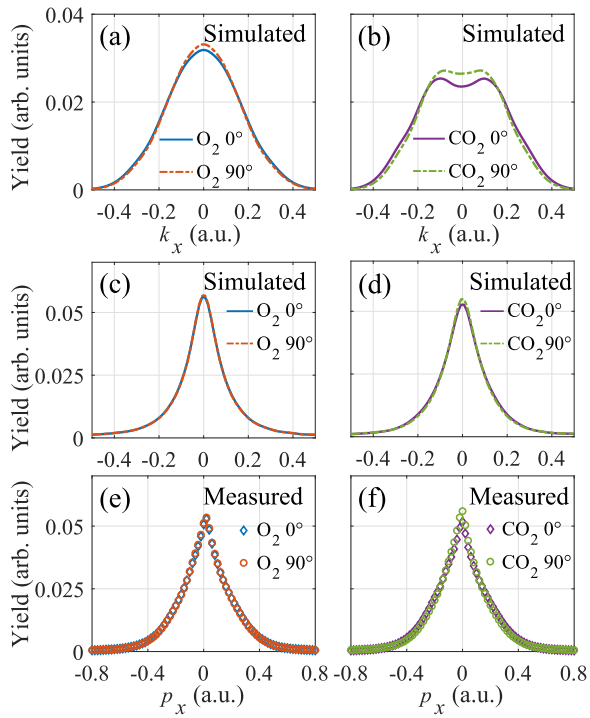

FIG. 5. (a)–(d) The simulated initial [(a) and (b)] and final [(c) and (e)] momentum distributions in the laser propagation direction of the linearly polarized laser field. (e) and (f) The same as (c) and (d) but for the measured results. The solid lines (diamonds) and the dash-dotted lines (circles) correspond to the alignment cases of $\theta = 0^\circ$ and $\theta = 90^\circ$, respectively.

the electron emission angle of $\phi = 90^\circ$ in the polarization plane according to the time-to-momentum mapping relation, i.e., $\mathbf{p} \approx -\mathbf{A}(t)$. Here, ϕ is the electron emission angle in the polarization plane relative to the p_z direction. $\phi = 90^\circ$ means that the electron is released along the positive p_y direction. The electron released at the instant deviating from the field peak will achieve an emission angle deviating from $\phi = 90^\circ$ in the polarization plane, which corresponds to a small absolute value of p_y. As a result, the peak of the p_y momentum distribution for $\theta = 0^\circ$ is larger than that for $\theta = 90^\circ$, as indicated by the dashed lines in Figs. 3(b) and 3(c). Further considering the Coulomb effect, the momentum distributions in the polarization plane are deflected by the Coulomb potential. For the alignment case of $\theta = 0^\circ$, the absolute value of p_y corresponding to the maximum of the PMD is still larger than that of $\theta = 90^\circ$, as shown in Figs. 3(d) and 3(e). Therefore the ND ($M_{\theta=0^\circ} - M_{\theta=90^\circ}$) shows two maxima at $|p_y| \approx 0.5$ a.u. along the p_y direction, which is consistent with the result in Fig. 1(g). Thus the ionization time distribution of the photoelectron is significantly affected by the molecular orbital, which is recorded by the PMDs. The ionization time distributions of CO_2 are very similar to those of O_2 for both $\theta = 0^\circ$ and $\theta = 90^\circ$. Therefore the ND of CO_2 also shows two maxima at $|p_y| \approx 0.5$ a.u. along the p_y direction, as shown in Fig. 1(h).

We next study the PMD along the laser propagation direction of the elliptically polarized laser fields. Along this direction, the momentum distributions of O_2 and CO_2 reveal a clear difference, which is induced by their different electronic structures. In the partial Fourier-transform approach, the influence of molecular electronic structures on the PMDs is mainly determined by the cut of the three-dimensional wave function at the matching point [28]. In Figs. 4(a)–4(d), we show the three-dimensional electronic wave functions of O_2 and CO_2 and their cuts at the matching point at the instant corresponding to the maximum of the laser field. As shown in Figs. 4(a) and 4(b), the difference of the electronic wave functions at the matching point between $\theta = 0^\circ$ and $\theta = 90^\circ$ of the O_2 molecule is very small. Thus the final momentum distributions of O_2 are similar for $\theta = 0^\circ$ and $\theta = 90^\circ$. The yield at $\theta = 0^\circ$ is a little higher than that at $\theta = 90^\circ$, as shown in Fig. 4(e). This is consistent with our measured result, as shown in Fig. 4(f). Therefore there is only one maximum at $p_x = 0$ in the p_x direction. Compared with O_2, CO_2 has a larger equilibrium O-O distance, and the wave function is more elongated in the direction of the molecular axis. Thus the wave functions of CO_2 at the matching point for $\theta = 0^\circ$ and $\theta = 90^\circ$ reveal a comparably larger difference, as shown in Figs. 4(c) and 4(d), which leads to very different final momentum distributions for $\theta = 0^\circ$ and $\theta = 90^\circ$. As shown in Figs. 4(g) and 4(h), the yield at $\theta = 0^\circ$ is higher than that at $\theta = 90^\circ$ when $|p_x| < 0.1$ a.u., and conversely, the yield at $\theta = 90^\circ$ is higher than that at $\theta = 0^\circ$ when $|p_x| > 0.1$ a.u. This leads to the minimum at $p_x \approx 0$ in the p_x direction for the ND of CO_2. Therefore the tiny difference between the molecular orbitals of O_2 and CO_2 can be identified from the PMDs using an elliptically polarized laser field.

In order to reveal the underlying mechanism of the similar patterns in the linearly polarized laser field for O_2 and CO_2 [Figs. 1(e) and 1(f)], we further study the initial momentum distribution at the tunnel exit and final momentum distribution along the laser propagation direction for O_2 and CO_2 molecules. Obviously, there are clear differences between $\theta = 0^\circ$ and 90° in the initial momentum distribution at the tunnel exit of both molecules, as shown in Figs. 5(a) and 5(b). However, the differences become small in the final momentum distributions, as shown in Figs. 5(c) and 5(d). Moreover, one can see that the final momentum distributions become much narrower compared with the initial momentum distributions. Those are consistent with our measured results, as shown in Figs. 5(e) and 5(f). The narrowing of the final momentum distribution comes from the Coulomb focusing effect [36,37]. Due to the Coulomb focusing effect, the difference of the molecular orbitals is obscured by the narrowed momentum distributions in the linearly polarized laser. Therefore, in the linearly polarized laser field, it is difficult to distinguish two similar electronic structures from the PMD. In the elliptically polarized laser field, as shown in Figs. 4(e) and 4(g), the final momentum distribution is wider than that in the linearly polarized laser field. This means that the Coulomb focusing effect is weaker in the elliptically polarized laser field. As a result, the tiny difference of the molecular orbital between O_2 and CO_2 can be identified from the PMD.

IV. CONCLUSION

In summary, we have distinguished two similar molecular orbitals of O_2 and CO_2 from the PMDs using an elliptically polarized laser field. By comparing the momentum distribution in the plane perpendicular to the major axis of the elliptically polarized laser field for O_2 and CO_2, we find that the PMDs reveal very different features for those two molecules. However, the NDs show similar patterns for O_2 and CO_2 in a linearly polarized laser field. This is because the Coulomb focusing effect is much stronger in the linearly polarized laser field, which masks the difference of the molecular orbitals between those two molecules. We find that the ionization time distribution of the electron is significantly affected by the electronic structures of the molecule, which can be directly observed from the PMDs in the elliptically polarized laser field. Our study provides an alternative way to probe molecular orbitals with a high resolution.

ACKNOWLEDGMENTS

This work is supported by the National Key Research and Development Program of China (Grant No. 2019YFA0308300) and the National Natural Science Foundation of China (Grant No. 12021004). The computation was completed in the HPC Platform of Huazhong University of Science and Technology.

[1] J. Muth-Böhm, A. Becker, and F. H. M. Faisal, Phys. Rev. Lett. **85**, 2280 (2000); **96**, 039902(E) (2006).
[2] Z. Y. Lin, X. Y. Jia, C. L. Wang, Z. L. Hu, H. P. Kang, W. Quan, X. Y. Lai, X. J. Liu, J. Chen, B. Zeng, W. Chu, J. P. Yao, Y. Cheng, and Z. Z. Xu, Phys. Rev. Lett. **108**, 223001 (2012).
[3] T. Zuo and A. D. Bandrauk, Phys. Rev. A **52**, R2511(R) (1995).
[4] L. Blackburn and M. Keller, Sci. Rep. **10**, 18449 (2020).
[5] M. Meckel, D. Comtois, D. Zeidler, A. Staudte, D. Pavičić, H. C. Bandulet, H. Pépin, J. C. Kieffer, R. Dörner, D. M. Villeneuve, and P. B. Corkum, Science **320**, 1478 (2008).
[6] C. I. Blaga, J. Xu, A. D. DiChiara, E. Sistrunk, K. Zhang, P. Agostini, T. A. Miller, L. F. DiMauro, and C. D. Lin, Nature (London) **483**, 194 (2012).
[7] K. Amini, M. Sclafani, T. Steinle, A.-T. Le, A. Sanchez, C. Müller, J. Steinmetzer, L. Yue, J. R. M. Saavedra, M. Hemmer, M. Lewenstein, R. Moshammer, T. Pfeifer, M. G. Pullen, J. Ullrich, B. Wolter, R. Moszynski, F. J. G. de Abajo, C. D. Lin, S. Gräfe *et al.*, Proc. Natl. Acad. Sci. USA **116**, 8173 (2019).
[8] D. Comtois, H.-C. Bandulet, M. Spanner, D. Pavičić, M. Meckel, D. Zeidler, H. Pépin, R. Dörner, J.-C. Kieffer, D. M. Villeneuve, P. B. Corkum, and A. Staudte, J. Mod. Opt. **60**, 1395 (2013).
[9] Q. Ji, S. Cui, X. You, X. Gong, Q. Song, K. Lin, H. Pan, J. Ding, H. Zeng, F. He, and J. Wu, Phys. Rev. A **92**, 043401 (2015).
[10] I. Petersen, J. Henkel, and M. Lein, Phys. Rev. Lett. **114**, 103004 (2015).
[11] J. Wu, M. Magrakvelidze, L. P. H. Schmidt, M. Kunitski, T. Pfeifer, M. Schöffler, M. Pitzer, M. Richter, S. Voss, H. Sann, H. Kim, J. Lower, T. Jahnke, A. Czasch, U. Thumm, and R. Dörner, Nat. Commun. **4**, 2177 (2013).
[12] A. Khan, D. Trabert, S. Eckart, M. Kunitski, T. Jahnke, and R. Dörner, Phys. Rev. A **101**, 023409 (2020).
[13] J. Yan, W. Xie, M. Li, K. Liu, S. Luo, C. Cao, K. Guo, W. Cao, P. Lan, Q. Zhang, Y. Zhou, and P. Lu, Phys. Rev. A **102**, 013117 (2020).
[14] M. Yu, K. Liu, M. Li, J. Yan, C. Cao, J. Tan, J. Liang, K. Guo, W. Cao, P. Lan, Q. Zhang, Y. Zhou, and P. Lu, Light Sci. Appl. **11**, 215 (2022).
[15] D. Shafir, H. Soifer, C. Vozzi, A. S. Johnson, A. Hartung, Z. Dube, D. M. Villeneuve, P. B. Corkum, N. Dudovich, and A. Staudte, Phys. Rev. Lett. **111**, 023005 (2013).
[16] M. Li, Y. Liu, H. Liu, Q. Ning, L. Fu, Jie Liu, Y. Deng, C. Wu, L. Y. Peng, and Q. Gong, Phys. Rev. Lett. **111**, 023006 (2013).
[17] W. Xie, J. Yan, M. Li, C. Cao, K. Guo, Y. Zhou, and P. Lu, Phys. Rev. Lett. **127**, 263202 (2021).
[18] R. Dörner, V. Mergel, O. Jagutzki, L. Spielberger, J. Ullrich, R. Moshammer, and H. Schmidt-Böcking, Phys. Rep. **330**, 95 (2000).
[19] J. Ullrich, R. Moshammer, A. Dorn, R. Dörner, L. Ph. H. Schmidt, and H. Schmidt-Böcking, Rep. Prog. Phys. **66**, 1463 (2003).
[20] D. Pavičić, K. F. Lee, D. M. Rayner, P. B. Corkum, and D. M. Villeneuve, Phys. Rev. Lett. **98**, 243001 (2007).
[21] T. Seideman, J. Chem. Phys. **103**, 7887 (1995).
[22] J. Ortigoso, M. Rodriguez, M. Gupta, and B. Friedrich, J. Chem. Phys. **110**, 3870 (1999).
[23] T. Nubbemeyer, K. Gorling, A. Saenz, U. Eichmann, and W. Sandner, Phys. Rev. Lett. **101**, 233001 (2008).
[24] M. Li, J. W. Geng, H. Liu, Y. Deng, C. Wu, L. Y. Peng, Q. Gong, and Y. Liu, Phys. Rev. Lett. **112**, 113002 (2014).

[25] J. Liu, W. Chen, B. Zhang, J. Zhao, J. Wu, J. Yuan, and Z. Zhao, Phys. Rev. A **90**, 063420 (2014).
[26] B. Zhang, W. Chen, and Z. Zhao, Phys. Rev. A **90**, 023409 (2014).
[27] S. G. Walt, N. B. Ram, M. Atala, N. I. Shvetsov-Shilovski, A. von Conta, D. Baykusheva, M. Lein, and H. J. Wörner, Nat. Commun. **8**, 15651 (2017).
[28] R. Murray, W. K. Liu, and M. Yu. Ivanov, Phys. Rev. A **81**, 023413 (2010).
[29] R. Murray, M. Spanner, S. Patchkovskii, and M. Yu. Ivanov, Phys. Rev. Lett. **106**, 173001 (2011).
[30] P. Krause and H. B. Schlegel, J. Phys. Chem. Lett. **6**, 2140 (2015).
[31] M. D. Śpiewanowski and L. B. Madsen, Phys. Rev. A **91**, 043406 (2015).
[32] M. J. Frisch, G. W. Trucks, H. B. Schlegel, G. E. Scuseria, M. A. Robb, J. R. Cheeseman, G. Scalmani, V. Barone, B. Mennucci, G. A. Petersson, H. Nakatsuji, M. Caricato, X. Li, H. P. Hratchian, A. F. Izmaylov, J. Bloino, G. Zheng, J. L. Sonnenberg, M. Hada, M. Ehara *et al.*, *GAUSSIAN 09 (Revision D.01)* (Gaussian, Wallingford, CT, 2013).
[33] https://cccbdb.nist.gov/
[34] M. Li, J. W. Geng, M. Han, M. M. Liu, L. Y. Peng, Q. Gong, and Y. Liu, Phys. Rev. A **93**, 013402 (2016).
[35] M. Li, M. M. Liu, J. W. Geng, M. Han, X. Sun, Y. Shao, Y. Deng, C. Wu, L. Y. Peng, Q. Gong, and Y. Liu, Phys. Rev. A **95**, 053425 (2017).
[36] D. Comtois, D. Zeidler, H. Pépin, J. C. Kieffer, D. M. Villeneuve, and P. B. Corkum, J. Phys. B: At. Mol. Opt. Phys. **38**, 1923 (2005).
[37] A. Rudenko, K. Zrost, Th. Ergler, A. B. Voitkiv, B. Najjari, V. L. B. de Jesus, B. Feuerstein, C. D. Schröter, R. Moshammer, and J. Ullrich, J. Phys. B: At. Mol. Opt. Phys. **38**, L191 (2005).